JGR Solid Earth

RESEARCH ARTICLE
10.1029/2022JB026012

Pore Pressure Diffusion and Onset of Induced Seismicity

Scott M. Stokes[1], Shemin Ge[1], Megan R. M. Brown[2], Elizabeth A. Menezes[1,3], Anne F. Sheehan[1,3], and Kristy F. Tiampo[1,3]

[1]Department of Geological Sciences, University of Colorado Boulder, Boulder, CO, USA, [2]Department of Earth, Atmosphere and Environment, Northern Illinois University, DeKalb, IL, USA, [3]Cooperative Institute for Research in Environmental Sciences, University of Colorado Boulder, Boulder, CO, USA

Key Points:

- Pore pressure change between 0.007 and 0.03 MPa initiates the onset of induced seismicity on the Trinidad fault zone
- The basal sedimentary interval restricted pore pressure diffusion, limiting the impact of high-rate injection wells in the short term
- The depth varying permeability of crystalline basement effects the manner and magnitude of pore pressure diffusion into basement faults

Supporting Information:

Supporting Information may be found in the online version of this article.

Correspondence to:

S. M. Stokes,
scst5299@colorado.edu

Citation:

Stokes, S. M., Ge, S., Brown, M. R. M., Menezes, E. A., Sheehan, A. F., & Tiampo, K. F. (2023). Pore pressure diffusion and onset of induced seismicity. *Journal of Geophysical Research: Solid Earth*, *128*, e2022JB026012. https://doi.org/10.1029/2022JB026012

Received 10 NOV 2022
Accepted 31 JAN 2023

Author Contributions:

Conceptualization: Scott M. Stokes, Shemin Ge
Data curation: Scott M. Stokes
Formal analysis: Scott M. Stokes
Funding acquisition: Shemin Ge, Anne F. Sheehan, Kristy F. Tiampo
Investigation: Scott M. Stokes
Methodology: Scott M. Stokes
Supervision: Shemin Ge, Megan R. M. Brown, Anne F. Sheehan, Kristy F. Tiampo
Visualization: Scott M. Stokes

Abstract The Raton Basin of Southern Colorado and Northern New Mexico experienced a significant increase in seismicity over the last several decades, including two M5+ earthquakes. The increase in seismicity started soon after an increase in wastewater disposal associated with coal-bed methane production. Twenty-nine wastewater injection wells have operated in the Basin, with several high-rate injectors located within a kilometer of the most seismically active regions. We developed a pore pressure model to investigate the relationship between pore pressure diffusion and onset of induced seismicity, with an emphasis on the Trinidad fault zones. Our model indicates that sufficient pore pressure increase had accumulated on the northern extent of the Trinidad fault zone to induce seismicity at the time of early-stage seismic activity. The hydrogeologic architecture of the Basin played a key role in controlling pore pressure perturbation. The basal sedimentary interval with moderately low diffusivity restricted vertical pore pressure diffusion, creating a substantial lag time between wells becoming active and the expression of perturbation in the fault zones. The spatiotemporal relationship between early-stage seismicity and wastewater injection in conjunction with modeled pore pressures suggests that the early-stage seismicity in the Raton Basin was likely triggered by pore pressure diffusion.

Plain Language Summary In the Raton Basin, coal-bed methane production sparked the need for deep wastewater disposal starting in 1994. Prior to wastewater injection few earthquakes were recorded within its boundaries but a large increase in earthquakes has been recorded over the last several decades. Pore pressure increase, caused by the deep wastewater injection, is thought to be the reason for the increase in local earthquakes. We developed a model to estimate pore pressure increases on several fault zones that have recently exhibited increased earthquake frequency. We found that wastewater injection produced increases in pore pressure on the fault zones large enough to cause earthquakes. This suggests that increased seismicity is, at least in part, the result of pore pressure change caused by deep wastewater injection.

1. Introduction

Deep wastewater injection has been cited as a cause of induced seismicity since the 1960's Rocky Mountain Arsenal earthquakes (Healy et al., 1968) and is recognized as the most likely type of injection to induce seismicity (Weingarten et al., 2015). Several studies have shown that small magnitude stress changes (0.01–0.1 MPa) can perturb a critically stressed fault enough to cause failure (Reasenberg & Simpson, 1992; Stein, 1999). Wastewater injection has been shown to produce anthropogenic perturbation that exceeds the stress change needed to reactivate a critically stressed fault (e.g., Brown et al., 2017; Goebel et al., 2017; Hornbach et al., 2015; Keranen et al., 2014; Zhang et al., 2013).

Field and modeling studies have suggested that pore pressure diffusion (e.g., Hornbach et al., 2015; Hsieh & Bredehoeft, 1981; Keranen et al., 2014; Nakai, Weingarten, et al., 2017), poroelastic stress changes (e.g., Goebel et al., 2017; Segall & Lu, 2015; Zhai et al., 2019), and static stress changes (e.g., Brown & Ge, 2018), including that from aseismic slip (e.g., Guglielmi et al., 2015), all contribute to inducing seismicity. The relative significance of these mechanisms varies at different stages of the seismic sequence and for seismicity at difference distances from injection, but pore pressure is considered a primary trigger for initiating induced seismicity sequences (Chang & Segall, 2016; Ge & Saar, 2022; Segall & Lu, 2015). This study focuses on early-stage seismicity and the contribution of pore pressure changes. Pore pressure diffusion results in increased pore pressure along a critically stressed fault that reduces effective normal stress, bringing the fault closer to failure (Healy et al., 1968; Hubbert & Rubey, 1959). The basis of fault slip follows the Coulomb criterion (e.g., King et al., 1994) when the

Writing – original draft: Scott M. Stokes
Writing – review & editing: Scott M. Stokes, Shemin Ge, Megan R. M. Brown, Elizabeth A. Menezes, Anne F. Sheehan, Kristy F. Tiampo

state of effective stress on a fault is perturbed by pore pressure or/and the shear and normal stresses. In the case of injection induced seismicity, in the absence of tectonics that cause changes in shear and normal stresses and assuming faults are critically stressed (Townend & Zoback, 2000), pore pressure perturbation from injection becomes the perturbation factor (Ge & Saar, 2022). When critically stressed faults are close to injection wells, and there is a hydraulic connection between the injection interval and seismogenic zone, pore pressure diffusion has been cited as a dominant triggering mechanism (e.g., Chang & Segall, 2016; Goebel et al., 2017). In this study we relate pore pressure diffusion to early-stage seismicity in the Raton Basin where the seismically active regions are near the injectors (Figure 1). Early-stage seismicity is defined as the first magnitude 3+ earthquakes to be recorded on previously quiescent faults after injection has started.

The Raton Basin, located on the Colorado-New Mexico border (Figure 1), hosts both coal-bed methane extraction and wastewater injection. Coal-bed methane is exploited from the upper stratigraphy while wastewater injection is conducted over a kilometer deeper (Figure 2; Colorado Oil and Gas Conservation Commission (COGCC, 2020); New Mexico Oil Conservation Division (NMOCD, 2020)), separated by the ∼1 km thick Pierre shale (Baltz, 1965). Wastewater injection started in Colorado in 1994 and New Mexico in 1999; a total of twenty-nine injection wells have operated over the last several decades (COGCC, 2020; NMOCD, 2020). Injection predominantly targets the permeable sedimentary rock of the Dakota formation at ∼2 km below surface elevation (COGCC, 2020; NMOCD, 2020). Below the injection interval lies the Permian-Pennsylvania basal sedimentary units (Figure 2) that separates the injection interval from the Precambrian basement (Robinson et al., 1964). On average, the Precambrian basement is 3 km below surface elevation and contains normal faulting (Herrmann, 2020).

The Basin is located near the margin of an extensional stress field near the confluence of the N-S oriented extensional Rio Grande Rift and the E-W compressive stress field that occupies much of the central United States (Lund Snee & Zoback, 2020, 2022). Maximum horizontal stress orientations vary in the Raton Basin from NE-SW to NW-SE and is believed to be related to the Basin being located near two differing stress fields (Glasgow et al., 2021; Lund Snee & Zoback, 2020, 2022). Focal mechanisms (Table S1 in Supporting Information S1) predominantly support normal faulting (Barnhart et al., 2014; Herrmann, 2020; Nakai, Weingarten, et al., 2017; Wang et al., 2020). Starting in 2001, the Raton Basin experienced a significant increase in seismicity coinciding with an increase in wastewater injection (Figure 3). There was a 40-fold increase in M3.8+ earthquakes when comparing seismicity from 1970–July 2001 to August 2001–2013 (Rubinstein et al., 2014). Since the start of injection, seismicity has predominately been concentrated on three fault zones surrounded by injection wells (Figure 1). Two of the fault zones have recorded significant earthquake sequences. The Trinidad fault zone housed the August-September 2001 earthquake sequence and the August-September 2011 earthquake sequence (Rubinstein et al., 2014). The Vermejo Park fault zone is suggested to have housed the August-September 2005 earthquake sequence (Nakai, Weingarten, et al., 2017). The August-September 2001 sequence marked *t* start of the Basin's increased seismicity (Rubinstein et al., 2014). The sequence occurred on the northern extent of the Trinidad fault zone (N. Trinidad fault zone) and was highlighted by a magnitude 4.5 earthquake on 5 September 2001 (Figure 1). The August-September 2005 earthquake sequence occurred just south of the Colorado-New Mexico border. The sequence was highlighted by a magnitude 5.0 earthquake on 10 August 2005 and is believed to have occurred on the northern extent of the Vermejo Park fault zone (Nakai, Weingarten, et al., 2017). The August-September 2011 sequence occurred on the southern extent of the Trinidad fault zone (S. Trinidad fault zone) and was highlighted by a magnitude 5.3 earthquake on 23 August 2011, the largest earthquake in the Basin's recorded history.

Studies have attributed the Raton Basin's increase in seismicity to wastewater injection (Nakai, Weingarten, et al., 2017; Rubinstein et al., 2014); although a detailed analysis of seismicity from 2016 to 2020 indicates that earthquake—earthquake interaction may be more significant than pore pressure diffusion (Glasgow et al., 2021). Glasgow et al. (2021) suggested that earthquake sequences in the Raton Basin are initiated by anthropogenic perturbation from injection, but stored tectonic stress continues to drive the sequence through earthquake—earthquake interaction. The initiation of earthquake sequences from anthropogenic perturbation highlights the question: what is the relationship between pore pressure diffusion and early-stage induced seismicity?

Nakai, Weingarten, et al. (2017) found that sufficient pore pressure perturbation on the Vermejo Park fault zone between 2008 and 2010 had accumulated in the seismogenic zone to induce seismicity. This study, however, only focused on one of the fault zones and did not investigate early-stage seismicity when pore pressure diffusion was

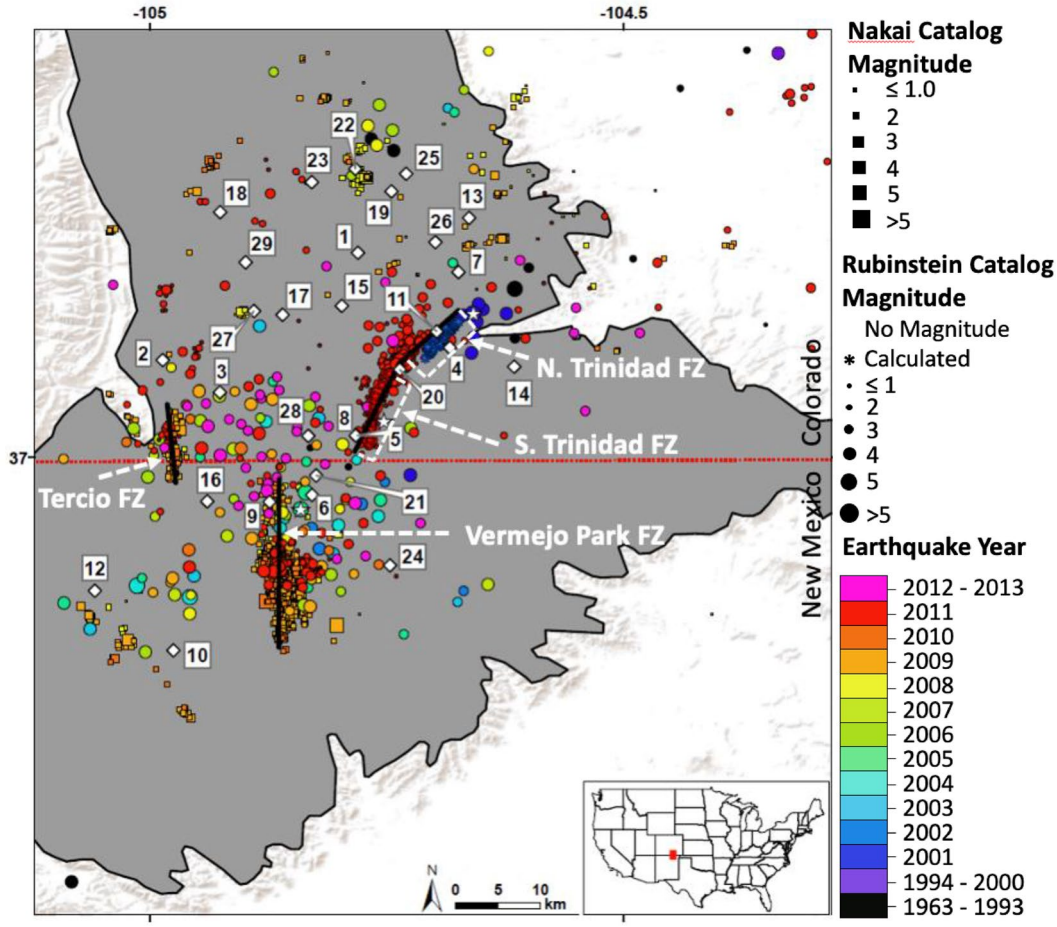

Figure 1. Study site location. Gray shaded area denotes Raton Basin. Wastewater disposal wells (white diamonds) labeled by age (1 = oldest well), Rubinstein et al. (2014) catalog of earthquakes from 1963–2013 colored by year and sized by earthquake magnitude (circles), Nakai, Sheehan, and Bilek (2017) catalog of earthquakes from 2008–2010 from the EarthScope Transportable array stations colored by year and sized by earthquake magnitude (squares), three studied fault zones (black lines).

likely the triggering mechanism before earthquake—earthquake interaction started. In this study we construct a numerical pore pressure model to determine a pressure value of early-stage seismicity, with a particular emphasis put on the *N*. Trinidad fault zone and the August-September 2001 earthquake sequence. Our model takes into consideration additional geologic detail that the previous model did not, such as the elevation variations of the relevant hydrostratigraphy. From this model we look to characterize what pore pressure increase initiated induced seismicity in the Raton Basin in hopes that our findings can assist in preliminary assessments of future wastewater injection sites.

2. Methods

2.1. Injection and Seismicity Data

Monthly injection rates for the wells in Colorado and New Mexico were collected from the Colorado Oil and Gas Conservation Commission (COGCC, 2020) and the New Mexico Oil Conservation Division (NMOCD, 2020), respectively. Injection between October 1999 and May 2006 was not reported for the New Mexico injection wells but water production was reported. Prior studies have shown that produced water from 1999 to 2006 can be used as a proxy for New Mexico's unreported injection (Nakai, Weingarten, et al., 2017; Rubinstein et al., 2014). We use the reported volume of produced water to estimate the approximate injection in New Mexico from 1999 to June 2006, additional information regarding how we specified injection can be found in Text S1 in Supporting Information S1.

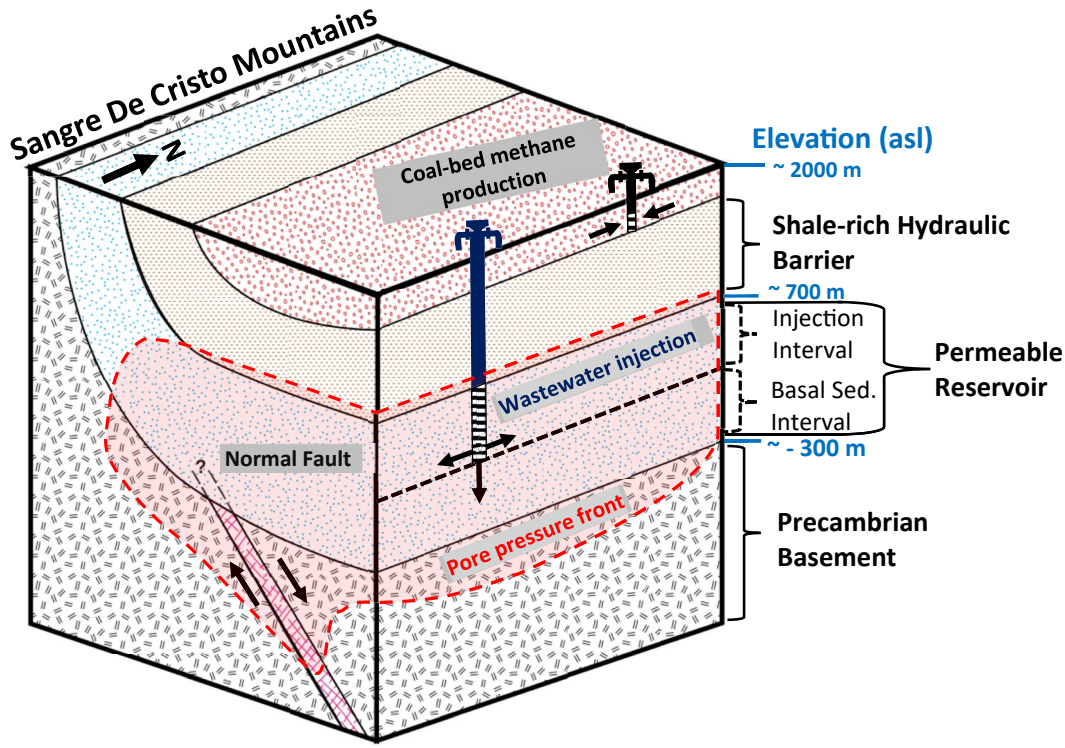

Figure 2. Schematic diagram showing the Basin geologic architecture, industrial activities, hydrostratigraphic classifications and pore pressure front (red shade). The diagram conceptualizes a critically stressed normal fault hydraulically connected to the permeable reservoir being perturbed by wastewater injection conducted stratigraphically above the seismogenic zone.

For this study we utilize two earthquake catalogs, the Rubinstein et al. (2014) catalog and the Nakai, Sheehan, and Bilek (2017) catalog. The Rubinstein et al. (2014) catalog contains earthquakes from 1963 to 2013 and incorporates the earthquakes recorded by the USGS temporary seismic networks deployed between September–October 2001 and August–December 2011. Most of the catalog has a horizontal uncertainty of 15 km because of the low-density seismic network in the region, with the exception of the earthquakes recorded by the temporary seismic networks which have horizontal uncertainties of 2 km for the 2001 deployment and 0.3 km for the 2011 deployment (Rubinstein et al., 2014). The Nakai, Sheehan, and Bilek (2017) catalog contains seismicity from 2008–2010 when the EarthScope Transportable Array was in the region. This catalog provides more accurate seismicity locations but only recorded earthquakes between 2008–2010 at a time when induced seismicity was already well-established throughout much of the Basin.

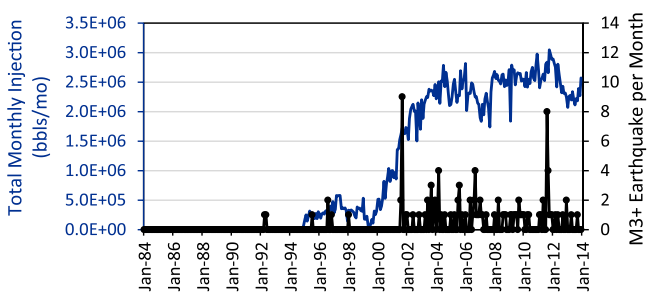

Figure 3. Comparison of total basin-wide monthly injection (blue line) and the number of magnitude 3+ earthquakes per month (black line) from the Rubinstein et al. (2014) catalog.

2.2. Conceptual Model

2.2.1. Structure Maps

To create a realistic representation of the Basin's subsurface hydrogeologic architecture, we based our model's hydrostratigraphy off Geldon (1989) and developed structure maps of the bottom of the shale-rich hydraulic barrier and top of the Precambrian basement (Figure S1 in Supporting Information S1). The structure maps were constructed using well lithology logs (COGCC, 2020; NMOCD, 2020), geologic maps (Baldwin & Muehlberger, 1959; Clark & Read, 1972; Fridrich et al., 2012; Garrabrant, 1993; Johnson, 1969, 1974, 1975; Lindsey, 1995a, 1995b, 1996; Pillmore, 2003; Vine, 1974; Wallace & Lindsey, 1996; Wanek et al., 1958) and Precambrian basement data (Hemborg, 1996). The stratigraphic data was interpolated using a natural neighbor algorithm to generate surfaces that encompasses the entire model domain. We then inserted the structure maps into the numerical model to represent subsurface elevation variations.

Table 1
Hydrostratigraphic Framework Hydraulic Diffusivities

Hydrostratigraphic unit	Homogeneous hydrostratigraphic framework diffusivities (m^2/s)[a]	Heterogeneous hydrostratigraphic framework diffusivities (m^2/s)[a]
Hydraulic barrier	10^{-8}	10^{-8}
Injection interval	0.1–10	0.1–10
Basal sedimentary interval	homogeneous permeable reservoir, no low-D basal sedimentary interval	0.01
Precambrian basement	Depth decaying (Figure 4a)	Depth decaying (Figure 4a)
Fault zones	0.01–1.0	0.01–1.0

[a]Value represent horizontal diffusivity values, vertical values are 1/10 of the horizontal values.

2.2.2. Faults

There are three prominent seismic lineations in the Raton Basin: the Trinidad fault zone, Vermejo Park fault zone and Tercio fault zone (Figure 1). In the hydrogeologic model we incorporate all three fault zones and assign hydrogeologic parameters that are different from the unfaulted Precambrian basement. Other studies have suggested that the fault zones are constructed of many small faults of variable strike and dip (Glasgow et al., 2021; Rubinstein et al., 2014) but modeling the exact geometry of the faults is outside the scope of this research. We are mainly concerned with how the fault contributes to vertical pore pressure diffusion into the basement. For that reason, the seismic lineations are simplified into three continuous zones each around 250 m wide, which is within the range of plausibility for a mature fault damage zone width (e.g., Savage & Brodsky, 2011). The strike, dip and depth of the three fault zones were determined based on a combination of the earthquake catalogs, moment tensors and knowledge of the regional stress regime. The orientations of the fault zones agree with the normal faulting observed in the Basin and with the regional east-west extensional stress regime (Herrmann, 2020). Specifics regarding the geometry of the fault zones can be found in the Text S1 in Supporting Information S1.

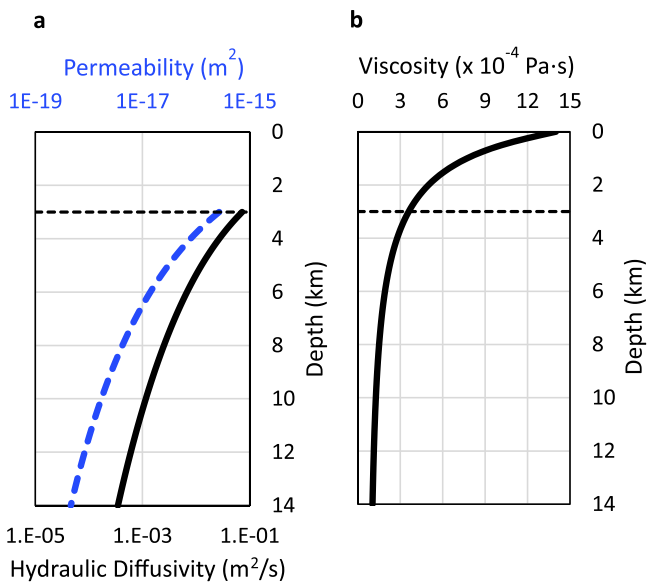

Figure 4. Vertical profiles showing the basement's depth decaying (a) permeability in blue (dashed), hydraulic diffusivity (S_s 1×10^{-7} 1/m) in black (solid) and (b) fluid viscosity. The dashed horizontal line represents the top of the basement.

2.3. Governing Equation

A three-dimensional numerical pore pressure model was developed for a heterogenous, anisotropic domain using MODFLOW-2005, a modular finite difference code developed by the USGS (Harbaugh et al., 2000). The code numerically solves the groundwater flow Equation 1 to simulate pore pressure diffusion caused by wastewater injection:

$$\frac{\partial}{\partial x}\left(K_{xx}\frac{\partial h}{\partial x}\right)+\frac{\partial}{\partial y}\left(K_{yy}\frac{\partial h}{\partial y}\right)+\frac{\partial}{\partial z}\left(K_{zz}\frac{\partial h}{\partial z}\right)+\sum_{n=1}^{N}Q_n(t)\delta(x-x_n)(y-y_n)(z-z_n)=S_s\frac{\partial h}{\partial t} \quad (1)$$

where h is hydraulic head (m), K_{xx}, K_{yy}, K_{zz} are the principle components of the hydraulic conductivity tensor (m/s), S_s is specific storage (m^{-1}), x, y, z are spatial coordinates, t is time (s), δ is the Dirac delta function (m^{-1}), Q_n is the injection rate for well n and N is the number of injection wells. As input into the model, monthly injection rates and details regarding well construction (Table S2 in Supporting Information S1) were extracted from the COGCC (2020) and NMOCD (2020) and combined with a range of hydraulic parameters (Table 1) that were collected from various sources discussed in more detail below.

2.4. Hydrogeologic Parameters

Hydraulic diffusivity is a hydrogeologic parameter used to describe pressure diffusion in a saturated porous medium. Diffusivity is equal to the ratio of hydraulic conductivity to specific storage:

$$D = \frac{K}{S_s} \tag{2}$$

where D is diffusivity (m^2/s), K is hydraulic conductivity (m/s) and S_s is specific storage (m^{-1}). When expressing the components of hydraulic conductivity and specific storage into Equation (2) it becomes apparent that diffusivity is a function of both medium and fluid properties (3) (Fetter, 2018):

$$D = \frac{k}{\mu(\alpha + n\beta)} \tag{3}$$

where k is permeability (m^2), μ is dynamic viscosity (Pa·s), n is porosity (dimensionless), α and β are rock and fluid compressibility (Pa^{-1}), respectively. Given the dependence of both medium and fluid properties, this study takes into consideration both pressure and temperature gradients.

2.4.1. Fluid Properties

Fluid composition and the effects of pressure and temperature on fluid viscosity are often not considered in modeling studies. The total dissolved solids (TDS) concentration of injection brine, if sufficiently larger than the TDS of the in-situ basement fluid, can cause density-driven flow of injection brine into the basement. The advection of injection brine results in increased pore pressure in the seismogenic zone even after injection has stopped (Pollyea et al., 2019, 2020). Additionally, fluid viscosity can change over an order of magnitude due to increased temperature over a large depth range, thus effecting the diffusivity of the medium.

Produced water from the Raton Basin has a relatively low TDS (~2800 ppm) and likely is not sufficient to produced density-driven brine flow (Blondes et al., 2018). The low TDS means transport of injection fluids is not enhanced by density variations between the injection fluid and the in-situ fluid making the pore pressure perturbation in the Raton Basin dominated by wellhead diffusion; therefore, we do not model the effects of fluid TDS. To incorporate the effects of increased pressure and temperature on diffusivity, we use a hydrostatic pressure gradient and geothermal gradient of 25°C/km to solve for fluid viscosity. Additional information can be found in Text S1 in Supporting Information S1.

2.4.2. Hydrostratigraphic Frameworks and Hydrogeologic Data

For much of the Basin's deep hydrostratigraphy, there is minimal locally recorded hydraulic conductivity and specific storage measurements that can be used to solve for diffusivity. To produce a range of diffusivities, the available data from the Raton Basin was coupled with hydrogeologic data from basins with similar hydrostratigraphy. The diffusivities were combined into two hydrostratigraphic frameworks, one with a homogeneous permeable reservoir and another with a heterogeneous permeable reservoir (Table 1). The homogeneous framework assumes the permeable reservoir is homogeneous with hydrogeologic properties representative of the injection interval. The heterogeneous framework divides the permeable reservoir into the injection interval and basal sedimentary interval (Figure 2). The spatial coverage, thickness and hydrogeologic properties of the basal sedimentary interval (Pennsylvanian and older) is uncertain. In the Raton Basin, the Permian-Pennsylvania Sangre de Cristo formation has been reported to unconformably overlay the Precambrian basement (Robinson et al., 1964). Cores taken from the Sangre de Cristo Formation, extracted within the basin, suggest permeabilities between 10^{-16}–10^{-15} m^2 (Bohlen, 2013). The resulting diffusivity is around 0.001–0.01 m^2/s. These estimates incorporate a viscosity that is adjusted for a temperature and pressure (81°C and 30 MPa) consistent with the average depth of the base of the formation (3 km, Figure 4). The heterogenous framework used the same injection interval diffusivities as the homogeneous framework but assigned the basal sedimentary interval, approximately 500 m thick, a diffusivity of 0.01 m^2/s (Table 1).

A shale-rich hydraulic barrier overlies the injection interval (Figure 2) and consists of the Pierre Shale, Niobrara Formation and Benton Formation. The hydraulic barrier was simplified into a single unit with hydrogeologic characteristics representative of the Pierre Shale. The hydraulic barrier was assigned a diffusivity of 10^{-8} m^2/s in all model simulations based on parameters derived from a field scale osmosis study (Garavito et al., 2006) and adjusted for a temperature and pressure of approximately 50°C and 18 MPa, respectively.

The injection interval consists of multiple geologic units that are simplified into a single hydrostratigraphic unit. A single injection recovery step rate test conducted in the Raton Basin backed out permeabilities for the Dakota formation and Entrada Sandstone (upper portion of the injection interval) ranging from 5.8×10^{-14} to

8.9×10^{-14} m^2 (Hernandez & Weingarten, 2019). To further determine a range of hydrogeologic parameters for the injection interval, we utilized additional data from hydrologic field testing, lab-based core analyses and calibrated models from proxy locations (Bredehoeft et al., 1983; Gries et al., 1976; Teeple et al., 2021). Permeabilities for the Dakota formation derived from proxy locations are similar to those measured in the Raton Basin. The hydraulic conductivities, when adjusted for a temperature and pressures corresponding to the depth of the injection interval (70°C and 25 MPa), are 1.4×10^{-6}–2.1×10^{-6} m/s. The corresponding diffusivities, when using the average specific storage from proxy locations ($\sim 1 \times 10^{-6}$ m^{-1}), are 1.4–2.1 m^2/s. Given uncertainties associated with determining hydraulic conductivity and specific storage, we use a range of diffusivities for the injection interval between 0.1 and 10 m^2/s (Table 1).

Directly measured hydrogeologic properties of Precambrian basement are scarce, but basement permeability has been shown to decrease as a function of depth causing significant heterogeneity over large depth ranges (Kuang & Jiao, 2014; Manning & Ingebritsen, 1999; Saar & Manga, 2004). To represent the basement's heterogeneous diffusivity, we took into consideration depth dependent viscosity (Huber et al., 2009; Wagner & Pruß, 2002) and used a depth decaying permeability function Equation (4) from Kuang and Jiao (2014):

$$\log k = \log k_r + (\log k_s - \log k_r)(1 + z)^{-\alpha} \tag{4}$$

where k is permeability (m^2), k_r is the residual permeability at depth (m^2), k_s is the permeability at zero depth (m^2), z is the depth (km) and α is the decay index (dimensionless). As seen in Figure 4, the basement's diffusivity decays with depth from ~0.07 m^2/s at the top of the basement (~3 km deep) to ~0.007 m^2/s when 3 km below the basement top (~6 km deep).

Within the basement we modeled three fault zones that are hydraulically connected to the permeable reservoir. The three faults were assigned bulk diffusivities that ranged from 0.01 to 1 m^2/s to simulate a range of fault characteristics from a low diffusivity sealing fault to a high diffusivity conductive fault. The range of diffusivities was established based on data collected from a tidal response study (Xue et al., 2013), lab-based core analyses of fault gouge and damage zone (Ree et al., 2018) and values used in similar hydro-mechanical models (Goebel et al., 2017; Nakai, Weingarten, et al., 2017; Yeo et al., 2020; Zhang et al., 2013).

2.5. Model Discretization and Boundary Conditions

The model domain dimensions are 130 km × 200 km x 11–14 km (depth) (Figure S2 in Supporting Information S1). The domain was discretized into approximately 5.5 million cells with horizontal discretization being 250 × 250 m in the injection and faulted regions and 1 × 1 km cells in the outer reaches of the model. The model was vertically discretized into 53 layers of varying thickness to accommodate fluctuating topography of lithological units. The hydraulic barrier was discretized into 6 layers with layer thickness decreasing with depth. The permeable reservoir was discretized into 12 layers with an average thickness of ~100 m. The basement was divided into 35 layers with an average thickness of ~250 m. The size of the model domain was designed to minimize boundary effects on the no flow boundary conditions assigned to the lateral and bottom boundaries of the model. The top of the model domain was made an open boundary.

3. Results

A numerical pore pressure model was developed to investigate the relationship between wastewater injection and increased seismicity. Two hydrostratigraphic frameworks were developed to represent the Raton Basin's subsurface hydrogeologic architecture, one with a homogeneous permeable reservoir and another with a heterogeneous permeable reservoir with the basal sedimentary interval being assign a low diffusivity of 0.01 m^2/s. Model simulations were run on both frameworks for a range of diffusivities for the injection interval and fault zones (Table 1). Based on the data discussed in Methods, the heterogeneous permeable reservoir was the most reasonable representation of the Basins subsurface hydrogeologic architecture. In the following subsections we present modeled pore pressure increases from the heterogeneous model framework to investigate the spatiotemporal relationship between pore pressure diffusion, early-stage seismicity, and high-rate injection wells. We include model results from all scenarios except those generated using an injection interval diffusivity of 0.1 m^2/s because

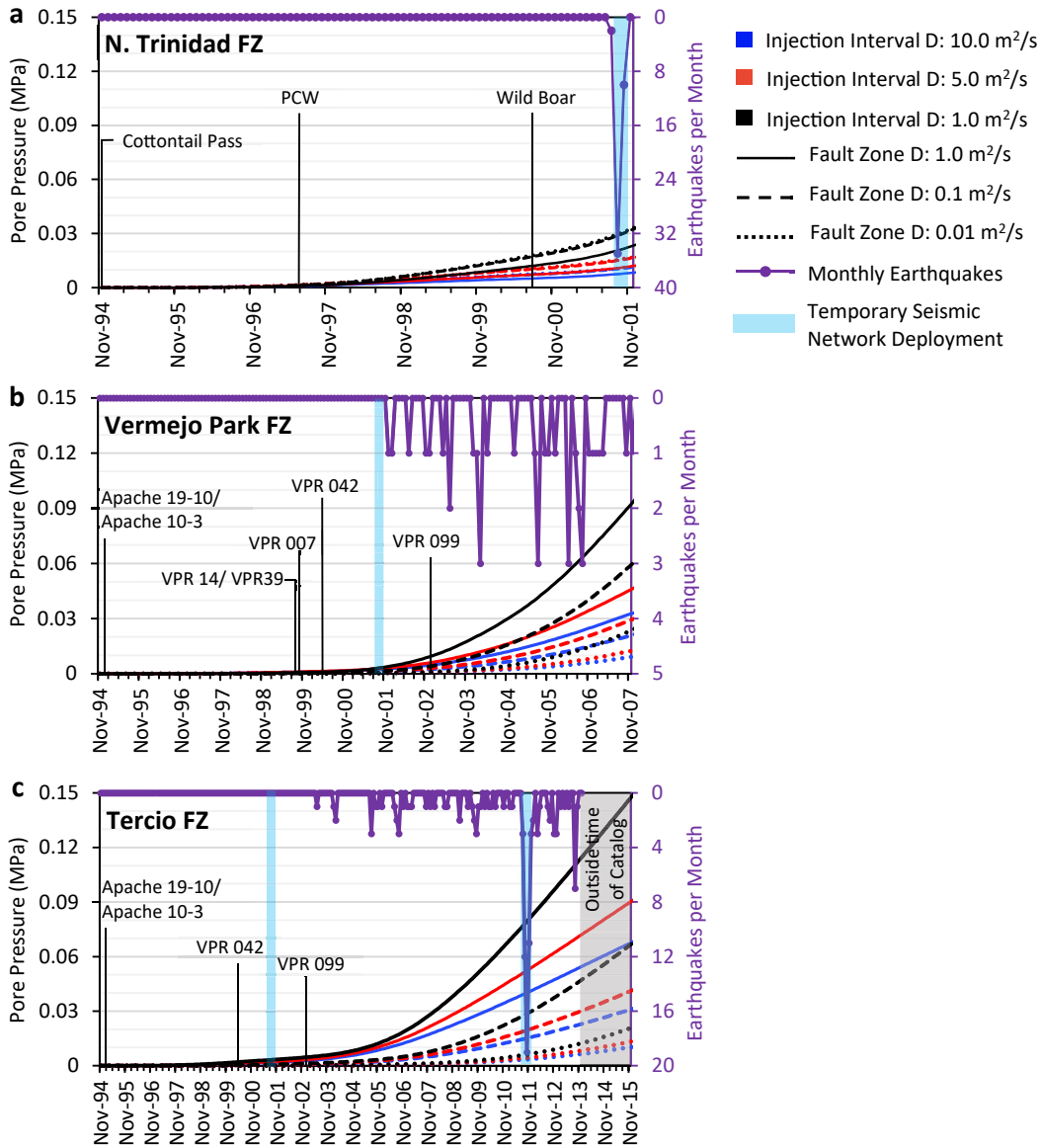

Figure 5. Modeled pore pressure change on each fault zone, located at white dots in panel (a), compared to monthly earthquakes within 15 km of the fault zone from the Rubinstein et al. (2014) catalog. Vertical black lines denote when a significant injection well became active and vertical translucent blue strips signifies when the USGS temporary seismic networks were active. (a) Modeled pore pressure at 3 km deep at a single location on the N. Trinidad fault zone. (b) Modeled pore pressure at 4 km deep at a single location on the Vermejo Park fault zone. (c) Modeled pore pressure at 5 km deep at a single location on the Tercio fault zone.

it produced unreasonably high pore pressure increases at the well that do not agree with underpressure estimates and wellhead pressures or lack thereof. More information regarding parameter constraining can be found in Text S2 in Supporting Information S1.

3.1. N. Trinidad Fault Zone: Seismicity, Pore Pressure and Injection

The August–September 2001 earthquake sequence marked the first occurrence of induced seismicity within the Raton Basin. The earthquakes sequence occurred along the northern portion of the Trinidad fault zone (N. Trinidad fault zone), a fault zone that was previously quiescent (Figure 5a). The earthquake sequence included 11 M3+ earthquakes between 28 August and 21 September 2001. The temporary seismic network recorded

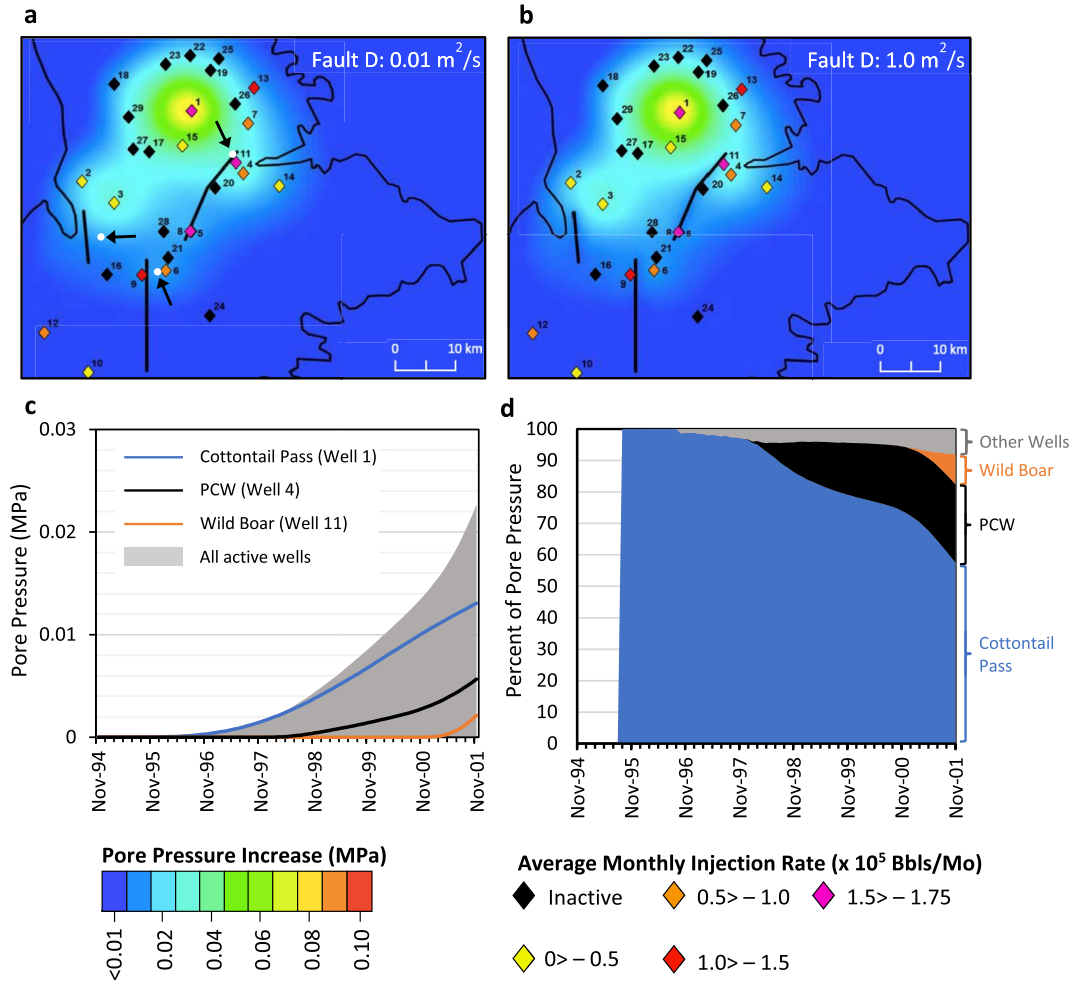

Figure 6. (a, b) Map view of modeled pore pressure perturbation at 3 km deep as of 1 September 2001 when using an injection interval diffusivity of 1.0 m^2/s with a (a) sealing fault zone or a (b) conductive fault zone. The diamonds represent the locations of the injection wells with colors corresponding to the average injection rate of the wells prior to September 2001 and labeled with the wells age number (1 = oldest well). The location of the fault zones at the top of the basement are denoted by the black lines. (c, d) Contribution to pore pressure change on the N. Trinidad fault zone at 3 km deep as of 1 September 2001 from the Cottontail Pass well (blue), PCW well (black) and the Wild Boar well (orange). (c) Comparison of total pore pressure change from all active wells (gray) to pore pressure change caused by the three individual wells. (d) Percent that the three wells contributed to total pore pressure change generated by all active wells.

additional earthquakes in September and October, but the earthquakes were either <M3 or did not have a magnitude calculated. Most of the seismicity associated with the 2001 sequence occurred around 3 km deep near the sedimentary-basement interface (Meremonte et al., 2002; Rubinstein et al., 2014). Modeled pore pressure increases at 3 km deep, as of 1 September 2001, ranged between 0.007 and 0.03 MPa (Figures 5a, 6a, 6b). When projecting seismicity from September 2001 onto a cross section of pore pressure diffusion all the seismicity falls within an area of pore pressure increase of 0.01 MPa or greater when modeling with an injection interval diffusivity of 1.0 m^2/s, regardless of fault zone diffusivity (Figure S3 in Supporting Information S1).

Pore pressure perturbation on the *N*. Trinidad fault zone was negligible until early 1998, after which pore pressure continued to rise at an increasing rate as additional injection wells started becoming active (Figure 5a). Early perturbation on the *N*. Trinidad Fault was caused by the Cottontail Pass injection well (well 1), located just over 10 km northwest of the fault zone (Figures 5a and 6a–6c). The Cottontail Pass injection well started injecting in November 1994 and had the second highest average monthly injection rate prior to the August-September 2001 earthquake sequence (Figure S4 and Table S3 in Supporting Information S1). The highest rate injection well at this time was the Wild Boar injection well (well 11), located within a kilometer of the N. Trinidad fault zone

(Figure 6a, Figure S4 and Table S3 in Supporting Information S1). The well began injecting in August 2000 but pore pressure perturbation caused by the well was not observed in the fault zone until mid 2001 (Figure 6c). Additional perturbation on the fault zone was caused by the PCW well (Well 4), located approximately 2.5 km southeast of the fault zone (Figure 6a). The PCW well became active in July 1997 and injected at low to moderate rates until March 2001 when it started injecting at higher rates (Figure S4 and Table S3 in Supporting Information S1).

3.2. Vermejo Park Fault Zone: Pore Pressure, Seismicity, and Injection

The Vermejo Park fault zone is located just south of the Colorado-New Mexico border in the center of the Basin (Figure 1). Seismicity started to migrate into this portion of the Basin as early as December 2001 and has remained highly active (Figure 5b). Within a 15 km radius of the northern extent of the fault zone, 16 earthquakes were recorded before the August-September 2005 earthquake sequence, 14 of which were M3+. The exact location and depth of early-stage seismicity in this portion of the Basin is uncertain because of the low-density seismic network. Additionally, injection rates for the New Mexico wells had to be estimated because operators in New Mexico did not start reporting injection rates until June 2006. The uncertainty of the seismicity and injection data makes correlating pore pressure and early-stage seismicity more ambiguous than on the *N*. Trinidad fault zone.

The catalog from Nakai, Sheehan, and Bilek (2017), which contains seismicity from 2008 to 2010, indicates that there are high concentrations of earthquakes on the Vermejo Park fault zone between 3 and 10 km deep with an average depth between 4 and 5 km, this is corroborated by nearby moment tensors from Herrmann (2020). Modeled pore pressure at the Vermejo Park fault zone was continuously monitored at 3 km deep (top of the fault zone) and 4 km deep. As of December 2001 and August 2005, pore pressure increase at 3 km deep ranged between 0.005–0.02 MPa and 0.03–0.2 MPa, respectively (Figure S5 in Supporting Information S1). At 4 km deep, as of December 2001 and August 2005, pore pressure increase ranged between 0–0.004 MPa and 0.003–0.04 MPa, respectively (Figure 5b).

Modeled pore pressure first became elevated on the northern portion of the fault zone, where most of the injection wells are located (Figures 6a and 6b). Pore pressure on the northern extent of the fault zone increased gradually until early 2001 when pore pressure started to increase at an elevated rate (Figure 5b, and Figure S4 in Supporting Information S1). The initial pore pressure perturbation was likely caused by the Apache 10-3 (well 2) and Apache 19-10 (well 3) but these wells were not high-rate injectors; so the initial perturbation was small (Figure 5b, Figure S4 in Supporting Information S1). When pore pressure started increasing at an elevated rate multiple high-rate injectors had been injecting for at least 8 months (Figure 5b, Figure S4 in Supporting Information S1). The closest wells are VPR 042 (well 9) and VPR 007 (well 6), located 0.6 and 3 km from the northern extent of the fault zone, respectively (Figure 6a). Both wells are estimated to have injected at moderately high to high rates and likely accounted for much of the perturbation on the fault zone (Figure 5b, Figure S4 and Table S3 in Supporting Information S1). Two additional high-rate injectors, VPR 39 (well 8) and VPR 99 (well 16), also contributed to pore pressure perturbation but are located 9 and 6.5 km from the fault zone, respectively (Figure 6a).

3.3. Tercio Fault Zone: Pore Pressure, Seismicity, and Injection

The Tercio fault zone is located on the Colorado-New Mexico border on the western side of the Basin (Figure 1). Seismicity started to occur within 15 km of the fault zone as early as June 2003 (Figure 5c). The Nakai, Sheehan, and Bilek (2017) catalog indicates that there are high concentrations of earthquakes between 3 and 7 km, while nearby moment tensors from Herrmann (2020) predominantly range in depth between 3 and 5 km. Modeled pore pressure at the Tercio fault zone was continuously monitored at approximately 3 km (top of fault zone) and 5 km deep. As of June 2003, modeled pore pressure at 3 km deep ranged between 0.007 and 0.02 MPa (Figure S5 in Supporting Information S1). At 5 km deep, as of June 2003, modeled pore pressure increase ranged between 0 and 0.005 MPa (Figure 5c).

Pore pressure gradually increased on the Tercio fault zone until mid 2003 when pore pressure started to increase at an elevated rate (Figure 5c, Figure S4 in Supporting Information S1). The initial perturbation was likely caused by wells Apache 10-3 (well 2) and Apache 19-10 (well 3). Both wells are within 5 km of the fault zone but have predominantly injected at low rates (Figure 6a, and Figure S4 in Supporting Information S1). As additional

high-rate injection wells (VPR 007 (well 6), VPR 042 (well 9), VPR 99 (well 16) and VPR 39 (well 8)) started injecting the rate of pore pressure change increased (Figure 5c, Figure S4 in Supporting Information S1). The two closest high-rate injectors are VPR 99 and VPR 042, located 4 and 9 km from the fault zone, respectively (Figure 6a). Unlike the other two fault zones, the Tercio fault zone is located farther away from high-rate injectors so there is a larger lag time between the start of injection and the expression of perturbation in the fault zone.

4. Discussion

4.1. N. Trinidad Fault Zone: August–September 2001 Earthquake Sequence

The August–September 2001 earthquake sequence represents the onset of induced seismicity in the Raton Basin with a M3.4 earthquake on 28 August 2001. Earthquake sequences in the Raton Basin have been characterized by initial earthquakes being triggered by anthropogenic perturbation while subsequent earthquakes are the result of stored tectonic stress and earthquake—earthquake interactions (Glasgow et al., 2021). The 28 August 2001 earthquake was likely triggered by pore pressure diffusion from nearby injection wells. Modeled pore pressure change at this time ranged between 0.007 and 0.03 MPa. When constraining modeled pore pressure to the scenarios that only used an injection interval diffusivity of 1.0 m^2/s, which is the diffusivity closest to that estimated for the Basin's injection formations, modeled pore pressure ranges from 0.02 to 0.03 MPa. This range of pore pressure increase is in agreement with previously suggested triggering thresholds for induced seismicity in other regions (e.g., Hornbach et al., 2015; Keranen et al., 2014; Ogwari et al., 2018), although, the hydrogeologic parameters that government pore pressure change are highly uncertain and are spatially variable so constraining an exact pore pressure change is not feasible. Additionally, injection volumes were estimated for the New Mexico wells prior to June 2006, although, at this time Colorado injection wells accounted for 87% of basin-wide injection and injection in New Mexico had only been going for two years so pore pressure change on the Trinidad fault zone caused by New Mexico wells is minimal (Figure 6d).

Prior to the 2001 earthquake sequence, 15 wells had been injecting in the Raton Basin. Three of the injection wells are responsible for 92% of the pore pressure accumulation on the *N*. Trinidad fault zone as of 1 September 2001 (Figure 6d). The three wells include the Cottontail Pass (well 1), PCW (well 4), and Wild Boar (well 11). The Wild Boar well had the highest average injection rate at the time (Table S3 in Supporting Information S1) and is located within a kilometer of the fault zone. It was previously suggested to be the most significant well in inducing the 2001 earthquake sequence (Rubinstein et al., 2014) but our model indicates that it accounted for only 7% of pore pressure increase on the *N*. Trinidad fault zone as of 1 September 2001 (Figure 6d). The PCW well, located ∼2.5 km southeast of the fault zone, accounted for 24% of the pore pressure increase. The Cottontail Pass well, located ∼10 km northwest of the fault zone, is responsible for 61% of the pore pressure perturbation.

The high injection rate and proximity of the Wild Boar well to the *N*. Trinidad fault zone made it an obvious well to attribute blame for triggering the 2001 earthquake sequence, but what was not considered before was the hydrogeology of the Basin. The basal sedimentary interval has a moderately low permeability (Bohlen, 2013) which restricts pore pressure diffusion into the basement and creates a lag time between the start of injection and expression of perturbation in the basement. Additionally, the Wild Boar well had only been injecting for 1 year, whereas the PCW well had been injecting for over 4 years and the Cottontail Pass well had been injecting for just under 7 years (Figure 5a). The combination of the low permeability basal sedimentary interval and the short duration of injection limited the Wild Boar wells contribution to pore pressure perturbation on the N. Trinidad fault zone. From this analysis, the most significant well in inducing the 2001 earthquake sequence was likely the Cottontail Pass well. This becomes interesting when considering the average injection rate of the Cottontail Pass well (∼166,000 bbls/mo; Table S3 in Supporting Information S1) is well below the average rate of some high-rate injection wells (300,000 + bbls/mo) in other regions, such as Oklahoma (e.g., Goebel et al., 2017; Keranen et al., 2014). This highlights that wells injecting at moderate rates over time can contribute significant enough pore pressure perturbation to induced seismicity on critically stressed faults even if it is not in close proximity.

4.2. Vermejo Park and Tercio Fault Zones

Given the data we have, the exact timing of early-stage seismicity is unknown based on earthquake catalogs alone. As an alternative we assumed the pore pressure value for initiating early-stage seismicity on the Vermejo and Tercio fault zones are similar to the pressure value established for the August-September 2001 earthquake

sequence. For all three fault zones to be reactive by the same degree of pore pressure increase seems unlikely. However, Glasgow et al. (2021) found that the fault zones are composed of many sub-faults of varying strike and dip. This suggests that each fault zone has fault segments that are optimally oriented for failure. The rock composition of the faults also is similar, given that seismicity predominantly occurs in the basement (Nakai, Weingarten, et al., 2017). Additionally, at the time of early-stage seismicity, the earthquake catalogs have large spatial uncertainties (15 km), which makes correlating early-stage seismicity with specific fault zones difficult. We were able to reliably do this for the *N*. Trinidad fault zone because a temporary seismic network was deployed shortly after the basins first induced earthquakes occurred in August 2001. The temporary network greatly enhanced our understanding of where and when seismicity was happening in the *N*. Trinidad fault zone, but the network was removed before the Vermejo Park and Tercio fault zones became reactivated. In the following we compare seismicity to the timing in which the Vermejo Park and Tercio fault zones reached 0.02 MPa of pore pressure change when modeling an injection interval diffusivity of 1.0 m^2/s.

At the average depth on seismicity (~4 km), the Vermejo Park fault zone reached 0.02 MPa of pore pressure increase on February 2004, April 2005, and July 2007 (Figure 5b). The timing was dependent on the fault zone diffusivity, with the earliest time corresponding with a conductive fault zone (1.0 m^2/s) and the latest time corresponding with a sealing fault zone (0.01 m^2/s). Prior to February 2004, April 2005, and July 2007, the Rubinstein et al. (2014) catalog recorded 9 earthquakes, 15 earthquakes, and 36 earthquakes within the 15 km of the fault zone, respectively. Additionally, the scenario that used a sealing fault zone did not surpass 0.02 MPa or pore pressure increase until after the August-September 2005 earthquake sequence. This sequence is considered to be the latest possible time that represents early-stage seismicity on the Vermejo Park fault zone.

At the average depth of seismicity (~5 km), the Tercio fault zone reached 0.02 MPa of pore pressure increase on January 2007, July 2010, and September 2015. Like the Vermejo Park fault zone the timing was dependent on fault zone diffusivity. Prior to January 2007 and July 2010, the Rubinstein et al. (2014) catalog recorded 17 earthquakes and 39 earthquakes within 15 km of the fault zone, respectively. Even more earthquakes were recorded before September 2015, but the Rubinstein catalog only includes earthquakes through 2013. The Nakai, Sheehan, and Bilek (2017) catalog first recorded seismicity on the Tercio fault zone on 17 July 2008, well before the intermediate diffusivity and sealing fault zones reached 0.02 MPa of pore pressure increase.

Both fault zones reached 0.02 MPa of pore pressure increase years after seismicity started being recorded within 15 km of the fault zones. It seems unlikely that even the earliest time in which 0.02 MPa of pore pressure increase was reached represents the timing of early-stage seismicity on either fault zone. This may indicate that early-stage seismicity occurred at shallower depths, closer to the sedimentary-basement interface. It also could be the result of local hydrogeologic heterogeneity that was not represented in the model, such as a fault zone that penetrates the basal sedimentary interval. Additionally, the injection rates for New Mexico wells are an estimate, because operators were not required to report injection rates until May 2006. This accumulation of unknowns prohibits us from precisely deducing the date of early-stage seismicity on the Vermejo Park and Tercio fault zones. On a broader scale, the spatiotemporal occurrence of seismicity is in agreement with modeled pore pressure diffusion. Seismicity first occurred on the *N*. Trinidad fault zone followed by the Vermejo Park fault zone and lastly the Tercio fault zone. Modeled pore pressure diffusion follows the same pattern, first becoming elevated on the *N*. Trinidad fault zone followed by the Vermejo Park and later the Tercio fault zone (Figure 7).

4.3. Additional Physical Mechanisms

While assuming that faults are critically stressed (Townend & Zoback, 2000) and focusing on changes in the state of stress is a common practice in studying induced seismicity, a more quantitative approach to assess the fault stability is the slip tendency analysis (Morris et al., 1996). Slip tendency is defined as the ratio of shear stress minus cohesion and effective normal stress on a fault. Such an analysis requires details of background stresses, fault orientation and frictional properties, as well as pore pressure. Shen et al. (2019) demonstrated such an application to hydraulic fracturing induced seismicity in western Canada. If the changes in background stresses and fault frictional properties are small, then pore pressure change is the main factor controlling slip tendency. In hydraulic fracturing operations where pore pressure changes are significant, often on par with or exceeding the hydrostatic pressure, slip tendency analysis is particularly useful and insightful (Moeck et al., 2009; Shen et al., 2019; Yaghoubi et al., 2022). In wastewater injection cases, however, the pressure changes are much smaller, and the resulting changes in slip tendency also are much smaller (e.g., Vacadda et al., 2021). For the

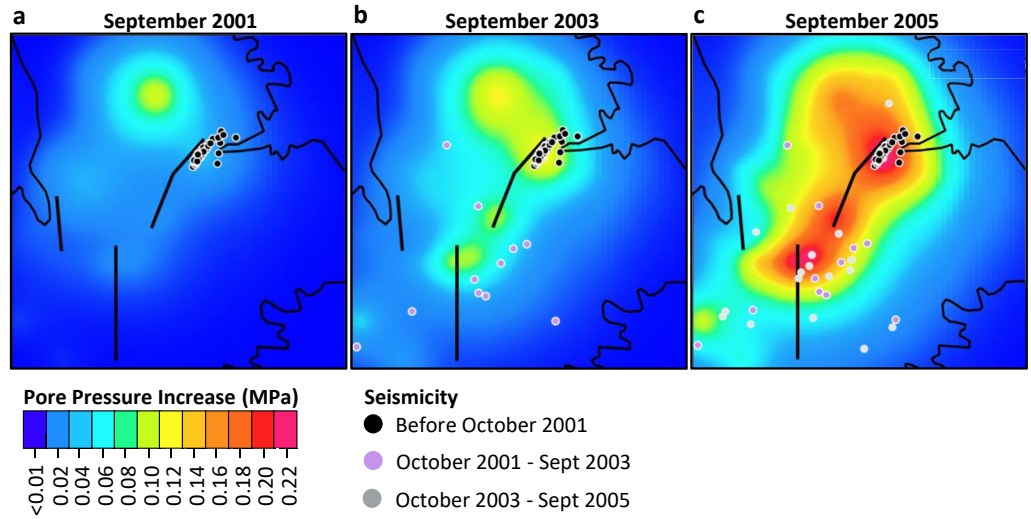

Figure 7. Pore pressure perturbation at the top of the basement (3 km deep) when modeling an injection interval diffusivity of 1.0 m^2/s and a sealing fault (0.01 m^2/s), the black lines represent the location of the fault zone at the top of the basement. (a) Pore pressure change as of September 2001 with seismicity recorded before October 2001 (black circles) projected onto the map of modeled pore pressure. (b) Pore pressure change as of September 2003 with seismicity recorded before October 2003 (purple circles) projected onto the map of modeled pore pressure. (c) Pore pressure change as of September 2005 with seismicity recorded before October 2005 (gray circles) projected onto the map of modeled pore pressure.

parameters in this study, analytical solution estimations (Rudnicki, 1986) suggest insignificant changes in slip tendency. Because this study focuses on pore pressure changes due to injection without a detailed background stress characterization, a detailed slip tendency analysis is beyond the scope of this analysis. Instead, we built on the assumption that the faults are critically stressed (Townend & Zoback, 2000) and a slight change in pore pressure could induce slip.

To examine the effects of poroelastic stress and compare them to pore pressure, we calculated the range of poroelastic stresses using the analytical solution of Rudnicki (1986, Equations 51 and 52). We used parameter values that would maximize the poroelastic effects. We simulated a single well using an injection rate of 2.5×10^6 bbls/month, which is over five times higher than the average basin-wide total monthly injection prior to September 2001 (Figure 3). We then calculated the poroelastic stresses at 1 km from the injection. We assumed three different fault angles to one of the principal stresses: 30°, 60°, and 90°, and used a uniform diffusivity range of 0.01–1.0 m^2/s. The results (Figure S6 in Supporting Information S1) show that the poroelastic stresses at the fault locations in most cases are much smaller than pore pressure changes. For the most extreme case of lowest diffusivity (0.01 m^2/s) and smallest fault angle (30°) poroelastic stresses exceeded pore pressure at the start of the injection when pore pressure has yet to build up. The poroelastic stresses and, more importantly, the resulting Coulomb stress on the faults are also small (<0.02 MPa).

Limited quantitative modeling for the Raton Basin exists. Nakai, Sheehan, and Bilek (2017) and Nakai, Weingarten, et al. (2017) presented a simplified pore pressure model that focused on pore pressure change along the Vermejo Park fault zone from 2008 to 2010. By 2008–2010 seismicity had already been well established in the basin and different triggering mechanisms, such as earthquake—earthquake interactions, likely controlled seismicity at this time. Early-stage seismicity is presumed to have been triggered by anthropogenic stress (Glasgow et al., 2021). The results of our modeling suggests that pore pressure change is most likely the predominant anthropogenic triggering mechanism for early-stage seismicity in the Raton Basin.

4.4. Sensitivity Analysis

Pore pressure modeling is known to be sensitive to hydrogeologic properties. In many cases, hydrogeologic properties of a Basin's deep hydrostratigraphy are relatively unconstrained. The lack of in situ pressure measurements limits our ability to calibrate these properties; it therefore is important to run sensitivity analyses to better

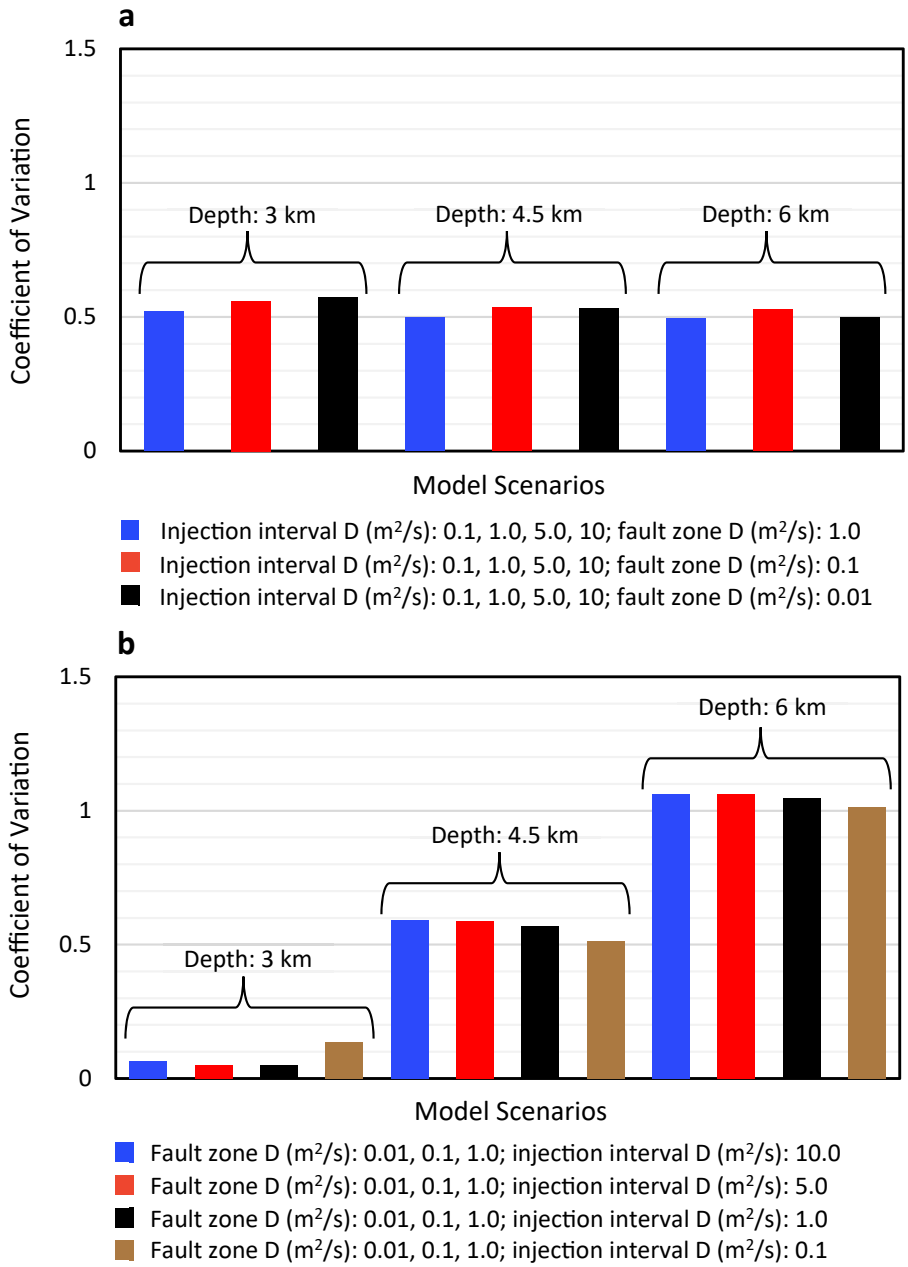

Figure 8. Coefficient of variation (CV, dimensionless) showing the pore pressure models sensitivity to varying the diffusivity of the injection interval and fault zones. The CV was calculated using modeled pore pressure for every month at 3, 4.5, and 6 km deep which was then averaged to produce a single value for each model scenario. (a) CV when varying injection interval diffusivity and keeping the fault zone diffusivity constant. (b) CV when varying the fault zone diffusivity but keeping the injection interval diffusivity constant.

understand how the modeled pore pressures may change with different hydrogeologic property scenarios. In the following we use the homogeneous hydrostratigraphic framework (Table 1), to examine how pore pressure perturbation changes when varying the diffusivity of the injection interval, fault zones and Precambrian basement.

4.4.1. Injection Interval Diffusivity Versus Fault Zone Diffusivity

The diffusivity of the injection interval and fault zones are crucial factors when modeling pore pressure diffusion into critically stressed faults. To evaluate the model's sensitivity to these parameters, we calculated the coefficient of variation (CV) for modeled pore pressure over a range of injection interval diffusivities (0.1–10 m^2/s) and fault

zone diffusivities (0.01–1.0 m^2/s). The CV is defined by CV = σ/μ, where σ is standard deviation and μ is mean. It is a measure of modeled pore pressure variability; the higher the CV the more sensitive the model is to the varied diffusivity. We calculated CV for two situations, (a) varying injection interval diffusivity but a constant fault zone diffusivity (Figure 8a, Table S4 in Supporting Information S1) (b) varying fault zone diffusivity but a constant injection interval diffusivity (Figure 8b, Table S4 in Supporting Information S1). We used monthly modeled pore pressure within the fault zone to calculate a monthly CV (CV time series) for each scenario at 3 km, 4.5 and 6 km deep (Figure S9 and Table S4 in Supporting Information S1). The CV time series were averaged to create a single CV value for each scenario at each depth (Figure 8). The number of months used to calculate the average CV was the same for all scenarios but the starting and ending times used were different. This is because the pore pressure front reached the monitoring depths at different times (Figure S9 in Supporting Information S1) and we wanted to make sure the same amount of time was used to calculate the average CV for all scenarios. For example, we calculated a CV per month at 3 km deep using four model simulations, all of which used a 1.0 m^2/s diffusivity fault zone but used different injection interval diffusivity (10, 5, 1, 0.1 m^2/s). The CV time series were averaged from December 1994 to August 2016 and represents modeled pore pressure variability at 3 km deep when varying the injection interval diffusivity with a constant 1.0 m^2/s fault zone diffusivity (Figure 8a, left most blue bar).

When varying the injection interval diffusivity with a constant fault zone diffusivity, CV only ranges between 0.49 and 0.57 (Figure 8a). When varying the fault zone diffusivity with a constant injection interval diffusivity, CV ranges between 0.05 and 1.06 (Figure 8b). The variable fault zone diffusivity situation led to a much wider range of CV and displays a depth trend with the highest CV at 6 km deep and the lowest CV at the 3 km depth (Figure 8b). Based on our analysis, fault zone diffusivity becomes more influential with increased depth into the basement and may become the governing parameter at several kilometers below the top of the basement. At an intermediate depth, pore pressure diffusion is significantly affected by both parameters. Near the sedimentary-basement interface, pore pressure diffusion is highly dependent on injection interval diffusivity with minimal dependence on fault zone diffusivity. When modeling pore pressure diffusion into basement, the hydrogeologic properties of both the injection interval and fault zones should be carefully considered.

4.4.2. Hydrogeologic Architecture of the Basement

The hydraulic properties of the basement are highly dependent on lithology and deformation history, but it is commonly cited that permeability of the basement decays with depth (Kuang & Jiao, 2014; Manning & Ingebritsen, 1999; Saar & Manga, 2004; Stober, 2011; Stober & Bucher, 2007). Stober and Bucher (2007) found that the crystalline basement, to several kilometers deep, has a hydraulic conductivity that averages around $10^{-8\pm1}$ m/s (permeability $\sim 5\times10^{-16\pm1}$ m^2). The corresponding diffusivity (assuming $S_s \sim 10^{-7}$ m^{-1}) is ~0.1 m^2/s.

Some hydro-mechanical studies choose to represent the basement as a homogeneous low diffusivity body ($D \leqq 0.0001$ m^2/s) (e.g., Fan et al., 2019; Norbeck & Horne, 2018; Tung et al., 2021; Zhai et al., 2019). Other studies, like this one, use a depth decaying permeability function to represent a basement that has a depth decaying diffusivity (e.g., Nakai, Weingarten, et al., 2017; Pollyea et al., 2019, 2020). The contrasting hydrogeologic representations of the basement raises the question what effect does basement diffusivity have on pore pressure diffusion into critically stressed faults? In the following, we compare the magnitude of modeled pore pressure change in a basement fault when using a homogeneous low diffusivity basement in contrast to a depth decaying diffusivity basement. The low diffusivity basement uses a homogeneous diffusivity of 0.0001 m^2/s while the depth decaying uses a diffusivity that decays from 0.07 m^2/s at the top of the basement to 0.0003 m^2/s at the bottom (Figure 4).

A homogeneous low diffusivity basement impedes vertical pore pressure diffusion into the unfaulted sections of the basement (Figure 9). The lack of vertical diffusion causes increased pore pressure perturbation in the sedimentary rock while also promoting lateral diffusion along the sedimentary-basement interface until reaching a fault zone which acts like a conduit for vertical pore pressure diffusion into the seismogenic zone (Figure 9). This allows for greater pore pressure build up along the entirety of the fault zones in all hydrogeologic scenarios with a conductive and intermediate diffusivity fault zone (Figure S10 in Supporting Information S1). When modeled with a sealing fault, the shallow portion of the fault zone (3 km deep) still experiences more pore pressure build up with the low diffusivity basement, but at intermediate and deep depths (4.5 and 6 km) the difference in pore pressure increase between the two basement types is relatively small (Figure 9, Figure S9 in Supporting Information S1). This likely occurs because the low diffusivity basement primarily diffuses pore pressure into the top of

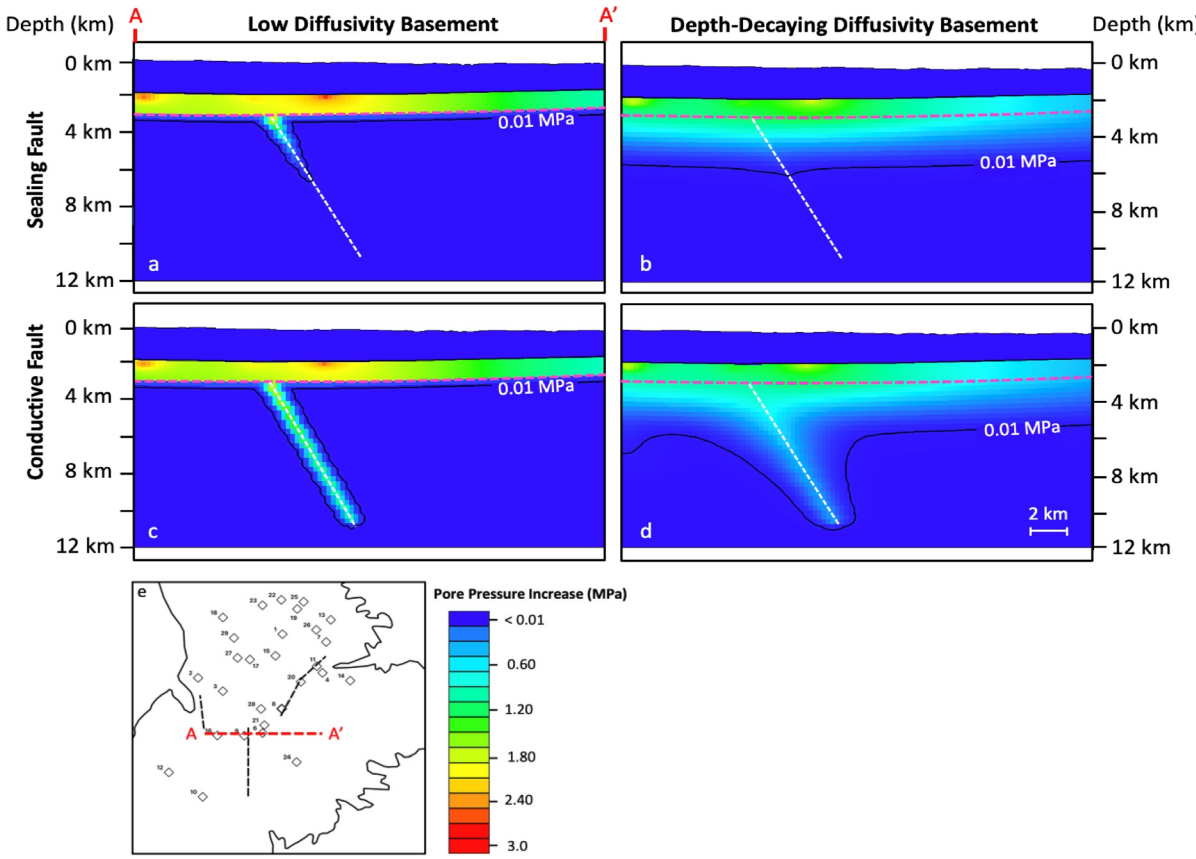

Figure 9. Comparison of pore pressure propagation into the basement when modeling a (a, c) homogeneous low diffusivity basement (D: 0.0001 m^2/s) and a (b, d) decaying diffusivity basement. An injection interval diffusivity of 1.0 m^2/s was used for all four plots, plots a and b used a sealing fault (D: 0.01 m^2/s) and plots c and d used a conductive fault (D: 1.0 m^2/s). The solid black line is a contour line of 0.01 MPa of pore pressure increase, the pink dashed line denotes the top of the basement and the white dashed line is the approximate centerline of the fault zone. (e) Map view showing the A–A' cross section location, faults (black dashed) and injection wells (diamonds).

the fault zone making pore pressure diffusion into deeper parts of the fault zone highly dependent on fault zone diffusivity. In contrast, the depth decaying basement allows pore pressure to diffuse into the unfaulted sections of the basement which allows pore pressure to diffuse into the fault zone from within the basement. This makes pore pressure perturbation at the intermediate and deeper depths less dependent on fault zone diffusivity when modeling a depth decaying basement.

Our analysis indicates that pore pressure diffusion into basement faults is substantially affected by basement diffusivity. In some scenarios the low diffusivity basement nearly tripled the amount of pore pressure increase that was produced by the depth decaying basement (Figure S10 in Supporting Information S1). Additionally, the low diffusivity basement primarily diffused pore pressure into the top of the fault zone regardless of fault zone diffusivity while the depth decaying basement allows for pore pressure to diffusion into the top of the fault zone and from within the basement. Given the sensitivity to basement diffusivity, future modeling should carefully consider the hydrogeologic properties of the basement.

5. Conclusion

Over the last several decades the Raton Basin has experienced a significant increase is seismicity that corresponded with an increase in wastewater injection. The recent seismicity has been concentrated on the Trinidad fault zone, Vermejo Park fault zone and Tercio fault zone. A numerical pore pressure model was used to relate pore pressure diffusion to onset of seismicity on these fault zones. We draw the following conclusions:

1. On a broad scale the spatiotemporal occurrence of early-stage seismicity is in agreeance with modeled pore pressure diffusion. Our model indicates that pore pressure first became elevated on the N. Trinidad fault zone followed by the Vermejo Park fault zone and lastly the Tercio fault zone. This pattern is similar to the migration of seismicity observed in the Raton Basin after injection started.
2. The initial seismicity of the August–September 2001 earthquakes sequence was likely triggered by pore pressure perturbation between 0.007 and 0.03 MPa. Three of the 15 active injection wells, Cottontail Pass, PCW and Wild Boar, produced 92% of the pore pressure change. The Cottontail Pass well produced a majority of the perturbation making it the most influential well in triggering the August–September 2001 earthquakes sequence, even though it was the furthest of the three wells from the fault zone. Closer wells produced less perturbation in the fault zone because they had been injecting for substantially less time and the basal sedimentary interval restricted vertical pore pressure diffusion, thus delaying pore pressure perturbation generated by these wells.
3. Given the available data, a precise date of early-stage seismicity could not be deduced for the Vermejo Park and Tercio fault zone, but it is very likely that the Vermejo Park fault zone was reactivated prior to the Tercio fault zone. At the average seismicity depths, the fault zones reached the estimated pressure value of initiating seismicity at a time that is likely too late to match the actual timing of early-stage seismicity. This could indicate early-stage seismicity was shallower than expected or there are hydrogeologic heterogeneities that allowed for enhanced pore pressure diffusion.
4. Model sensitivity to varying the diffusivity of the injection interval and fault zones suggest that diffusivity of the injection interval affects modeled pore pressure perturbation at all depths along the fault zone. The fault zone diffusivity plays a muted role at shallows depths but highly affects pore pressure perturbation at greater depths.
5. For most hydrogeologic scenarios the homogeneous low diffusivity basement produced substantially greater pore pressure perturbation within the fault zones than the depth decaying diffusivity basement. The homogeneous low diffusivity basement prohibited vertical pore pressure propagation into the unfaulted sections of the basement, concentrating pore pressure diffusion into the top of the fault zones. The depth decaying basement allowed pore pressure to propagate deeper into the unfaulted sections of the basement which allowed pore pressure diffusion into both the top and sides of the fault zones. When modeling a sealing fault zone pore pressure increase at moderate and deep depths was similar when comparing the two basement representations. This highlights that pore pressure perturbation in a fault zone is more dependent on fault zone diffusivity when modeling a homogenous low diffusivity basement. The hydrogeologic properties of the basement substantially affects pore pressure diffusion and should be considered in future hydro-mechanical models. Data

Conflict of Interest

The authors declare no conflicts of interest relevant to this study.

Data Availability Statement

Wastewater injection data for the wells located in the Colorado portion of the basin was retrieved from (COGCC, 2020; https://cogcc.state.co.us/data.html). Wastewater injection data for the wells located in the New Mexico portion of the basin was retrieved from (NMOCD, 2020; https://wwwapps.emnrd.state.nm.us/ocd/ocdpermitting/data/wells.aspx). Lithology logs used to create the structure maps were manually extracted from well files. Lithology logs from Colorado were retrieved from (COGCC, 2020; https://cogccmap.state.co.us/cogcc_gis_online/) using the interactive map application. Lithology logs from New Mexico were retrieved from (NMOCD, 2020; https://nm-emnrd.maps.arcgis.com/apps/webappviewer/index.html?id=4d017f2306164de29fd2fb9f8f35ca75) using the interactive map application. The Nakai, Sheehan, and Bilek (2017) earthquake catalog was retrieved from the Supporting Information of the Nakai, Sheehan, and Bilek (2017) paper. The Rubinstein et al. (2014) catalog was received from Justin Rubinstein but was reported to have been incorporated into the USGS ComCat catalog. An open-source software called MODFLOW was used to model pore pressure diffusion and can be retrieved from https://www.usgs.gov/mission-areas/water-resources/science/modflow-and-related-programs.

Acknowledgments
Funding for this research was provided in part by the United States Department of Energy Grant DE-SC0020222.

References

Baldwin, B., & Muehlberger, W. R. (1959). *Geologic Studies of Union County, New Mexico*. State Bureau of Mines and Mineral Resources, New Mexico Institute of Mining & Technology.

Baltz, E. H. (1965). Stratigraphy and history of the Raton basin and notes on San Luis basin, Colorado-New Mexico. *American Association of Petroleum Geologists Bulletin*, *49*, 2041–2075. https://doi.org/10.1306/a6633882-16c0-11d7-8645000102c1865d

Blondes, M. S., Gans, K. D., Engle, M. A., Kharaka, Y. K., Reidy, M. E., Saraswathula, V., et al. (2018). *U.S. Geological Survey National Produced Waters Geochemical Database (ver. 2.3, January 2018)*. U.S. Geological Survey data release. https://doi.org/10.5066/F7J964W8

Bohlen, K. (2013). Pre-exploration geothermal resource assessment for the Raton Basin, Colorado - The rest of the story. *GRC Transactions*, *37*, 933–940.

Bredehoeft, J. D., Neuzil, C. E., & Milly, P. C. D. (1983). Regional flow in the Dakota aquifer: A study of the role of confining layers (Vol. *2237*). USGS Water Supply Paper 223.

Brown, M. R., & Ge, S. (2018). Small earthquakes matter in injection-induced seismicity. *Geophysical Research Letters*, *45*(11), 5445–5453. https://doi.org/10.1029/2018gl077472

Brown, M. R., Ge, S., Sheehan, A. F., & Nakai, J. S. (2017). Evaluating the effectiveness of induced seismicity mitigation: Numerical modeling of wastewater injection near Greeley, Colorado. *Journal of Geophysical Research: Solid Earth*, *122*(8), 6569–6582. https://doi.org/10.1002/2017JB014456

Chang, K. W., & Segall, P. (2016). Injection-induced seismicity on basement faults including poroelastic stressing. *Journal of Geophysical Research: Solid Earth*, *121*(4), 2708–2726. https://doi.org/10.1002/2015JB012561

Clark, K. F., & Read, C. B. (1972). *Geology and ore deposits of Eagle Nest area*. New Mexico State Bureau of Mines and Mineral Resources.

Colorado Oil and Gas Conservation Commission. (2020). Colorado Oil and Gas Conservation Commission, COGCC website. Retrieved from http://cogcc.state.co.us/data.html#/cogis

Fan, Z., Eichhubl, P., & Newell, P. (2019). Basement fault reactivation by fluid injection into sedimentary reservoirs: Poroelastic effects. *Journal of Geophysical Research: Solid Earth*, *124*(7), 7354–7369. https://doi.org/10.1029/2018JB017062

Fetter, C. W. (2018). *Applied hydrogeology*. Waveland Press.

Fridrich, C. J., Shroba, R. R., & Hudson, A. M. (2012). Preliminary geologic map of the Big Costilla Peak area, Taos County, New Mexico, and Costilla County, Colorado. U. S. Geological Survey. Open-File Report OF-2012-1041.

Garavito, A. M., Kooi, H., & Neuzil, C. E. (2006). Numerical modeling of a long-term in situ chemical osmosis experiment in the Pierre Shale, South Dakota. *Advances in Water Resources*, *29*(3), 481–492. https://doi.org/10.1016/j.advwatres.2005.06.004

Garrabrant, L. A. (1993). *Water Resources of Taos County, New Mexico*. Open-File Report OF-93-4107 (Vol. 93(4107)). U. S. Geological Survey.

Ge, S., & Saar, M. O. (2022). Review: Induced seismicity during geoenergy development—A hydromechanical perspective. *Journal of Geophysical Research: Solid Earth*, *127*(3), e2021JB023141. https://doi.org/10.1029/2021JB023141

Geldon, A. L. (1989). Ground-water hydrology of the central Raton Basin, Colorado and New Mexico. *U. S. Geological Survey Water-Supply Paper*, *2288*, 1–81.

Glasgow, M., Schmandt, B., Wang, R., Zhang, M., Bilek, S. L., & Kiser, E. (2021). Raton Basin induced seismicity is hosted by networks of short basement faults and mimics tectonic earthquake statistics. *Journal of Geophysical Research: Solid Earth*, *126*(11), e2021JB022839. https://doi.org/10.1029/2021JB022839

Goebel, T. H., Weingarten, M., Chen, X., Haffener, J., & Brodsky, E. E. (2017). The 2016 Mw5.1 Fairview, Oklahoma earthquakes: Evidence for long-range poroelastic triggering at >40 km from fluid disposal wells. *Earth and Planetary Science Letters*, *472*, 50–61. https://doi.org/10.1016/j.epsl.2017.05.011

Gries, J. P., Rahn, P. H., & Baker, R. K. (1976). *A pump test in the Dakota Sandstone at Wall, south Dakota*. Science Center, University of South Dakota.

Guglielmi, Y., Cappa, F., Avouac, J. P., Henry, P., & Elsworth, D. (2015). Induced seismicity. Seismicity triggered by fluid injection-induced aseismic slip. *Science*, *348*(6240), 1224–1226. https://doi.org/10.1126/science.aab0476

Harbaugh, A. W., Banta, E. R., Hill, M. C., & Macdonald, M. G. (2000). The US geological survey modular ground water models: User guide to modularization concepts and the groundwater flow process. *US Geological Survey*, *121*.

Healy, J. H., Rubey, W. W., Griggs, D. T., & Raleigh, C. B. (1968). The Denver earthquakes. *Science*, *161*(3848), 1301–1310. https://doi.org/10.1126/science.161.3848.1301

Hemborg, H. T. (1996). *Basement structure map of Colorado with major oil and gas fields*. Colorado Geological Survey, Department of Natural Resources.

Hernandez, R., & Weingarten, M. (2019). Step-rate test calibration of primary injection reservoir permeability in a case of injection induced seismicity, Raton Basin, CO-NM. In *AGU fall meeting abstracts* (Vol. 2019, p. S13E-0493).

Herrmann, R. B. (2020). *North America moment tensor 1995–2020*. St. Louis University website. Retrieved from http://www.eas.slu.edu/eqc/eqc_mt/MECH.NA/

Hornbach, M. J., DeShon, H. R., Ellsworth, W. L., Stump, B. W., Hayward, C., Frohlich, C., et al. (2015). Causal factors for seismicity near Azle, Texas. *Nature Communications*, *6*(6728), 1–11. https://doi.org/10.1038/ncomms7728

Hsieh, P. A., & Bredehoeft, J. D. (1981). A reservoir analysis of the Denver earthquakes: A case of induced seismicity. *Journal of Geophysical Research*, *86*(B2), 903–920. https://doi.org/10.1029/JB086iB02p00903

Hubbert, M. K., & Rubey, W. W. (1959). Role of fluid pressure in mechanics of overthrust faulting: I. Mechanics of fluid-filled porous solids and its application to overthrust faulting. *The Geological Society of America Bulletin*, *70*(2), 115–166. https://doi.org/10.1130/0016-7606(1961)72[1445:ROFPIM]2.0.CO;2

Huber, M. L., Perkins, R. A., Laesecke, A., Friend, D. G., Sengers, J. V., Assael, M. J., et al. (2009). New international formulation for the viscosity of H2O. *Journal of Physical and Chemical Reference Data*, *38*(2), 101–125. https://doi.org/10.1063/1.3088050

Johnson, R. B. (1969). *Geologic map of the Trinidad quadrangle, south-central Colorado*. Open-File Report OF-558. U. S. Geological Survey.

Johnson, R. B. (1974). *Geologic map of the Fort Union quadrangle, Mora County, New Mexico*. Open-File Report OF-1164. U. S. Geological Survey.

Johnson, R. B. (1975). *Geologic map of the Rainsville quadrangle, Mora County, New Mexico*. Open-File Report OF-1276. U. S. Geological Survey.

Keranen, K. M., Weingarten, M., Abers, G. A., Bekins, B. A., & Ge, S. (2014). Sharp increase in central Oklahoma seismicity since 2008 induced by massive wastewater injection. *Science*, *345*(6195), 448–451. https://doi.org/10.1126/science.1255802

King, G. C., Stein, R. S., & Lin, J. (1994). Static stress changes and the triggering of earthquakes. *Bulletin of the Seismological Society of America*, *84*(3), 935–953. https://doi.org/10.1016/0148-9062(95)94484-2

Kuang, X., & Jiao, J. J. (2014). An integrated permeability-depth model for Earth's crust. *Geophysical Research Letters*, *41*(21), 7539–7545. https://doi.org/10.1002/2014GL061999

Lindsey, D. A. (1995a). *Geologic map of the Cuchara quadrangle, Huerfano County, Colorado*. Open-File Report OF-2283. U. S. Geological Survey.

Lindsey, D. A. (1995b). *Geologic map of the McCarty Park quadrangle, Costilla and Huerfano counties, Colorado*. Open-File Report OF-2282. U. S. Geological Survey.

Lindsey, D. A. (1996). *Reconnaissance geologic map of the Cucharas Pass quadrangle, Huerfano and Las Animas counties, Colorado*. Open-File Report OF-2294. U. S. Geological Survey.

Lund Snee, J. E., & Zoback, M. D. (2020). Multiscale variations of the crustal stress field throughout North America. *Nature Communications*, *11*(1), 1–9. https://doi.org/10.1306/08102120151

Lund Snee, J.-E., & Zoback, M. D. (2022). State of stress in areas of active unconventional oil and gas development in North America. *AAPG Bulletin*, *106*(2), 355–385. https://doi.org/10.1306/08102120151

Manning, C. E., & Ingebritsen, S. E. (1999). Permeability of the continental crust: Implications of geothermal data and metamorphic systems. *Reviews of Geophysics*, *37*(1), 127–150. https://doi.org/10.1029/1998RG900002

Meremonte, M. E., Lahr, J. C., Frankel, A. D., Dewey, J. W., Crone, A. J., Overturf, D., et al. (2002). *Investigation of an earthquake swarm near Trinidad, Colorado, August-October 2001 (No. 2002-73)*. Open-File Rept. 02-0073. US Geological Survey.

Moeck, I., Kwiatek, G., & Zimmermann, G. (2009). Slip tendency analysis, fault reactivation potential and induced seismicity in a deep geothermal reservoir. *Journal of Structural Geology*, *31*(10), 1174–1182. https://doi.org/10.1016/j.jsg.2009.06.012

Morris, A. P., Ferrill, D. A., & McGinnis, R. N. (1996). Using fault displacement and slip tendency to estimate stress states. *Journal of Structural Geology*, *83*, 60–72. https://doi.org/10.1016/j.jsg.2015.11.010

Nakai, J. S., Sheehan, A. F., & Bilek, S. L. (2017). Seismicity of the Rocky Mountains and Rio Grande Rift from the EarthScope transportable array and CREST temporary seismic networks, 2008–2010. *Journal of Geophysical Research: Solid Earth*, *122*(3), 2173–2192. https://doi.org/10.1002/2016JB013389

Nakai, J. S., Weingarten, M., Sheehan, A. F., Bilek, S. L., & Ge, S. (2017). A possible causative mechanism of Raton Basin, New Mexico and Colorado earthquakes using recent seismicity patterns and pore pressure modeling. *Journal of Geophysical Research: Solid Earth*, *122*(10), 8051–8065. https://doi.org/10.1002/2017jb014415

New Mexico Oil Conservation Division. (2020). New Mexico Oil and Conservation Division, 2016, permitting. Retrieved from https://wwwapps.emnrd.state.nm.us/ocd/ocdpermitting/data/wells.aspx

Norbeck, J. H., & Horne, R. N. (2018). Maximum magnitude of injection-induced earthquakes: A criterion to assess the influence of pressure migration along faults. *Tectonophysics*, *733*, 108–118. https://doi.org/10.1016/j.tecto.2018.01.028

Ogwari, P. O., DeShon, H. R., & Hornbach, M. J. (2018). The Dallas-Fort Worth airport earthquake sequence: Seismicity beyond injection period. *Journal of Geophysical Research: Solid Earth*, *123*(1), 553–563. https://doi.org/10.1002/2017JB015003

Pillmore, C. L. (2003). *Geologic map of the Vermejo Park quadrangle, Colfax County, New Mexico, and Las Animas County, Colorado*. Open-File Report OF-2003-438. U. S. Geological Survey.

Pollyea, R. M., Chapman, M. C., Jayne, R. S., & Wu, H. (2019). High density oilfield wastewater disposal causes deeper, stronger, and more persistent earthquakes. *Nature Communications*, *10*(1), 1–10. https://doi.org/10.1038/s41467-019-11029-8

Pollyea, R. M., Konzen, G. L., Chambers, C. R., Pritchard, J. A., Wu, H., & Jayne, R. S. (2020). A new perspective on the hydraulics of oilfield wastewater disposal: How PTX conditions affect fluid pressure transients that cause earthquakes. *Energy & Environmental Science*, *13*(9), 3014–3031. https://doi.org/10.1039/D0EE01864C

Reasenberg, P. A., & Simpson, R. W. (1992). Response of regional seismicity to the static stress change produced by the Loma Prieta earthquake. *Science*, *255*(5052), 1687–1690. https://doi.org/10.1126/science.255.5052.1687

Ree, J. H., Kim, J. H., Park, C., Kim, C. M., Han, R., Shimamoto, T., & Kang, H. C. (2018). Proxies for the 2017 Pohang earthquake fault and modelling of fluid flow. *AGU Fall Meeting Abstracts*, *2018*, S23B–0519.

Robinson, G. D. V., Wanek, A. A., Hays, W. H., & McCallum, M. E. (1964). *Philmont country: The rocks and landscape of a famous New Mexico ranch*. US Government Printing Office.

Rubinstein, J. L., Ellsworth, W. L., McGarr, A., & Benz, H. M. (2014). The 2001-present induced earthquake sequence in the Raton Basin of Northern New Mexico and southern Colorado. *Bulletin of the Seismological Society of America*, *104*(5), 2162–2181. https://doi.org/10.1785/0120140009

Rudnicki, J. W. (1986). Fluid mass sources and point forces in linear elastic diffusive solids. *Mechanics of Materials*, 5(4), 383–393. https://doi.org/10.1016/0167-6636(86)90042-6

Saar, M. O., & Manga, M. (2004). Depth dependence of permeability in the Oregon Cascades inferred from hydrogeologic, thermal, seismic, and magmatic modeling constraints. *Journal of Geophysical Research*, *109*(B4). https://doi.org/10.1029/2003JB002855

Savage, H. M., & Brodsky, E. E. (2011). Collateral damage: Evolution with displacement of fracture distribution and secondary fault strands in fault damage zones. *Journal of Geophysical Research*, *116*(B3), B03405. https://doi.org/10.1029/2010JB007665

Segall, P., & Lu, S. (2015). Injection-induced seismicity: Poroelastic and earthquake nucleation effects. *Journal of Geophysical Research: Solid Earth*, *120*(7), 5082–5103. https://doi.org/10.1002/2015JB012060

Shen, L. W., Schmitt, D. R., & Schultz, R. (2019). Frictional stabilities on induced earthquake fault planes at Fox Creek, Alberta: A pore fluid pressure dilemma. *Geophysical Research Letters*, *46*(15), 8753–8762. https://doi.org/10.1029/2019GL083566

Stein, R. S. (1999). The role of stress transfer in earthquake occurrence. *Nature*, *402*(6762), 605–609. https://doi.org/10.1038/45144

Stober, I. (2011). Depth-and pressure-dependent permeability in the upper continental crust: Data from the Urach 3 geothermal borehole, southwest Germany. *Hydrogeology Journal*, *19*(3), 685–699. https://doi.org/10.1007/s10040-011-0704-7

Stober, I., & Bucher, K. (2007). Hydraulic properties of the crystalline basement. *Hydrogeology Journal*, *15*(2), 213–224. https://doi.org/10.1007/s10040-006-0094-4

Teeple, A. P., Ging, P. B., Thomas, J. V., Wallace, D. S., & Payne, J. D. (2021). *Hydrogeologic framework, geochemistry, groundwater-flow system, and aquifer hydraulic properties used in the development of a conceptual model of the Ogallala, Edwards-Trinity (High Plains), and Dockum aquifers in and near Gaines, Terry, and Yoakum Counties, Texas (No. 2021-5009)*. US Geological Survey.

Townend, J., & Zoback, M. D. (2000). How faulting keeps the crust strong. *Geology*, *28*(5), 399–402. https://doi.org/10.1130/0091-7613(2000)28<399:HFKTCS>2.0.CO;2

Tung, S., Zhai, G., & Shirzaei, M. (2021). Potential link between 2020 Mentone, West Texas M5 earthquake and nearby wastewater injection: Implications for aquifer mechanical properties. *Geophysical Research Letters*, *48*(3), e2020GL090551. https://doi.org/10.1029/2020GL09055

Vadacca, L., Rossi, D., Scotti, A., & Buttinelli, M. (2021). Slip tendency analysis, fault reactivation potential and induced seismicity in the Val d'Agri oilfield (Italy). *Journal of Geophysical Research: Solid Earth*, *126*(1), e2019JB019185. https://doi.org/10.1029/2019JB019185

Vine, J. D. (1974). Geologic map and cross sections of the La Veta Pass, La Veta, and Ritter Arroyo Quadrangles, Huerfano and Costilla counties. (No. 833).

Wagner, W., & Pruß, A. (2002). The IAPWS formulation 1995 for the thermodynamic properties of ordinary water substance for general and scientific use. *Journal of Physical and Chemical Reference Data*, *31*(2), 387–535. https://doi.org/10.1063/1.1461829

Wallace, A. R., & Lindsey, D. A. (1996). *Geologic map of the Trinchera Peak quadrangle, Costilla, Huerfano, and Las Animas counties, Colorado*. Open-File Report OF-2312. U. S. Geological Survey.

Wanek, A. A., Read, C. B., Robinson, G. D., Hays, W. H., & McCallum, M. (1958). *Geologic map and geologic sections of Philmont Ranch quadrangle, New Mexico (No. 59-126)*. Open-File Report OF-425. U. S. Geological Survey.

Wang, R., Schmandt, B., Zhang, M., Glasgow, M., Kiser, E., Rysanek, S., & Stairs, R. (2020). Injection-induced earthquakes on complex fault zones of the Raton Basin illuminated by machine-learning phase picker and dense nodal array. *Geophysical Research Letters*, *46*(14), e2020GL088168. https://doi.org/10.1029/2020gl088168

Weingarten, M., Ge, S., Godt, J. W., Bekins, B. A., & Rubinstein, J. L. (2015). High-rate injection is associated with the increase in US mid-continent seismicity. *Science*, *348*(6241), 1336–1340. https://doi.org/10.1126/science.aab1345

Xue, L., Li, H. B., Brodsky, E. E., Xu, Z. Q., Kano, Y., Wang, H., et al. (2013). Continuous permeability measurements record healing inside the Wenchuan earthquake fault zone. *Science*, *340*(6140), 1555–1559. https://doi.org/10.1126/science.1237237

Yaghoubi, A., Dusseault, M. B., & Leonenko, Y. (2022). Injection-induced fault slip assessment in Montney Formation in Western Canada. *Scientific Reports*, *12*(1), 11551. https://doi.org/10.1038/s41598-022-15363-8

Yeo, I. W., Brown, M. R. M., Ge, S., & Lee, K. K. (2020). Causal mechanism of injection-induced earthquakes through the Mw 5.5 Pohang earthquake case study. *Nature Communications*, *11*(1), 1–12. https://doi.org/10.1038/s41467-020-16408-0

Zhai, G., Shirzaei, M., Manga, M., & Chen, X. (2019). Pore-pressure diffusion, enhanced by poroelastic stresses, controls induced seismicity in Oklahoma. *Proceedings of the National Academy of Sciences*, *116*(33), 16228–16233. https://doi.org/10.1073/pnas.1819225116

Zhang, Y., Person, M., Rupp, J., Ellett, K., Celia, M. A., Gable, C. W., et al. (2013). Hydrogeologic controls on induced seismicity in crystalline basement rocks due to fluid injection into basal reservoirs. *Groundwater*, *51*(4), 525–538. https://doi.org/10.1111/gwat.12071

References From the Supporting Information

Barnhart, W. D., Benz, H. M., Hayes, G. P., Rubinstein, J. L., & Bergman, E. (2014). Seismological and geodetic constraints on the 2011 Mw5. 3 Trinidad, Colorado earthquake and induced deformation in the Raton Basin. *Journal of Geophysical Research: Solid Earth*, *119*(10), 7923–7933. https://doi.org/10.1002/2014JB011227

Bucher, K., & Stober, I. (2010). Fluids in the upper continental crust. *Geofluids*, *10*(1-2), 241–253. https://doi.org/10.1111/j.1468-8123.2010.00279.x

Caine, J. S., Evans, J. P., & Forster, C. B. (1996). Fault zone architecture and permeability structure. *Geology*, *24*(11), 1025–1028. https://doi.org/10.1130/0091-7613(1996)024<1025:FZAAPS>2.3.CO;2

Eorc, J. (2016). ALOS global digital surface model "ALOS World 3D-30m"(AW3D30).

Kelley, S. A. (2015). Geothermal potential of the Raton Basin, New Mexico, New Mexico geological society. Guidebook 66 - Geology of the Las Vegas area. In *New Mexico geological society 66th annual fall field conference guidebook* (pp. 261–275).

Morgan, P. (2009). A preliminary analysis of geothermal resources in the central Raton Basin, Colorado, from bottom-hole temperature data. *Geothermal Resources Council - Transactions*, *33*, 509–513.

Nelson, P. H., Gianoutsos, N. J., & Anna, L. O. (2013). Outcrop control of basin-scale underpressure in the Raton Basin, Colorado and New Mexico. *Mountain Geologist*, *50*(2), 37–63.